Concurrent Inhibition of ERK and Farnesyltransferase Suppresses the Growth of HRAS Mutant Head and Neck Squamous Cell Carcinoma

Sehrish Javaid[1], Antje Schaefer[2,3], Craig M. Goodwin[3], Victoria V. Nguyen[3,4], Frances L. Massey[3,4], Mariaelena Pierobon[5], Da'Jhnae Gambrell-Sanders[4], Andrew M. Waters[3], Kathryn N. Lambert[3], J. Nathaniel Diehl[6], G. Aaron Hobbs[2,3], Kris C. Wood[7], Emanuel F. Petricoin III[5], Channing J. Der[1,2,3], and Adrienne D. Cox[1,2,3,8]

ABSTRACT

Human papilloma virus (HPV)-negative head and neck squamous cell carcinoma (HNSCC) is a common cancer worldwide with an unmet need for more effective, less toxic treatments. Currently, both the disease and the treatment of HNSCC cause significant mortality and morbidity. Targeted therapies hold new promise for patients with HPV-negative status whose tumors harbor oncogenic *HRAS* mutations. Recent promising clinical results have renewed interest in the development of farnesyltransferase inhibitors (FTIs) as a therapeutic strategy for *HRAS*-mutant cancers. With the advent of clinical evaluation of the FTI tipifarnib for the treatment of *HRAS*-mutant HNSCC, we investigated the activity of tipifarnib and inhibitors of HRAS effector signaling in HRAS-mutant HNSCC cell lines. First, we validated that HRAS is a cancer driver in HRAS-mutant HNSCC lines. Second, we showed that treatment with the FTI tipifarnib largely phenocopied HRAS silencing, supporting HRAS as a key target of FTI antitumor activity. Third, we performed reverse-phase protein array analyses to profile FTI treatment-induced changes in global signaling, and conducted CRISPR/Cas9 genetic loss-of-function screens to identify previously unreported genes and pathways that modulate sensitivity to tipifarnib. Fourth, we determined that concurrent inhibition of HRAS effector signaling (ERK, PI3K, mTORC1) increased sensitivity to tipifarnib treatment, in part by overcoming tipifarnib-induced compensatory signaling. We also determined that ERK inhibition could block tipifarnib-induced epithelial-to-mesenchymal transition, providing a potential basis for the effectiveness of this combination. Our results support future investigations of these and other combination treatments for HRAS mutant HNSCC.

Introduction

The three human RAS genes (*HRAS*, *KRAS*, and *NRAS*) comprise the most frequently mutated oncogene family in human cancer and are key targets for anticancer therapeutics (1). One approach to blocking RAS function is inhibition of membrane association. RAS proteins become activated and engage their downstream effectors at the inner leaflet of the plasma membrane. To achieve this required localization, they undergo a series of posttranslational modifications. The addition of a C15 farnesyl isoprenoid lipid to the C-terminal membrane targeting motif of RAS is the first and essential step in this process (2), catalyzed by the enzyme farnesyl transferase (FTase).

Two potent and selective FTase inhibitors (FTIs) that block transfer of farnesyl isoprenoids to RAS, tipifarnib (3) and lonafarnib (4), were advanced to phase III clinical evaluation for cancer treatment and found to be surprisingly nontoxic to normal tissues (5). Unfortunately, these trials were focused on the cancers with the highest frequencies of RAS mutations: pancreatic, colorectal, and non–small cell lung cancers, where the predominant mutated RAS isoform is KRAS. Preclinical studies had shown the ability of KRAS and NRAS, but not HRAS, to undergo alternative prenylation and thereby escape the effects of inhibition by FTIs (6). The dismal outcomes of these clinical trials greatly diminished interest in targeting RAS membrane association as an anti-RAS therapeutic strategy (5). The ability of FTIs to effectively inhibit HRAS membrane association suggested that HRAS-driven cancers would be susceptible to FTI treatment. However, the low frequency of HRAS mutations overall in cancer (3%) has long redirected overall anti-RAS drug discovery efforts to focus on KRAS.

The arrival of the era of precision medicine, where actionable targets can be identified even from low occurrence mutations, has altered this mindset. With FTIs already established as effective HRAS inhibitors, and already shown to be well tolerated, cancers harboring *HRAS* mutations have become of interest for clinical evaluation of FTIs. One such cancer is head and neck squamous cell carcinoma (HNSCC; ref. 7), a common cancer worldwide (8, 9) that affects critical functional structures such as the tongue, pharynx, and other parts of the oral cavity. Because of its anatomical locations and the consequences of

[1]Program in Oral and Craniofacial Biomedicine, University of North Carolina at Chapel Hill, Chapel Hill, North Carolina. [2]Department of Pharmacology, University of North Carolina at Chapel Hill, Chapel Hill, North Carolina. [3]Lineberger Comprehensive Cancer Center, University of North Carolina at Chapel Hill, Chapel Hill, North Carolina. [4]Department of Biology, University of North Carolina at Chapel Hill, Chapel Hill, North Carolina. [5]Center for Applied Proteomics and Molecular Medicine, Institute for Advanced Biomedical Research, George Mason University, Manassas, Virginia. [6]Curriculum in Genetics & Molecular Biology, University of North Carolina at Chapel Hill, Chapel Hill, North Carolina. [7]Department of Pharmacology and Cancer Biology, Duke University, Durham, North Carolina. [8]Department of Radiation Oncology, University of North Carolina at Chapel Hill, Chapel Hill, North Carolina.

Note: Supplementary data for this article are available at Molecular Cancer Therapeutics Online (http://mct.aacrjournals.org/).

Corresponding Authors: Adrienne D. Cox, Department of Radiation Oncology and Pharmacology, University of North Carolina at Chapel Hill, Lineberger Comprehensive Cancer Center, Chapel Hill, NC 27599. E-mail: adrienne_cox@med.unc.edu; and Channing J. Der, Department of Pharmacology, and Lineberger Comprehensive Cancer Center, University of North Carolina at Chapel Hill, Chapel Hill, NC 27599. E-mail: cjder@med.unc.edu

Mol Cancer Ther 2022;21:762–74

doi: 10.1158/1535-7163.MCT-21-0142

existing treatments, HNSCC causes significant mortality and morbidity. Conventional treatment options include surgery, radiation, and platinum chemotherapy, with more recent utilization of EGFR inhibitors and immunotherapy including PD-1 and PD-L1 inhibitors (10, 11). Yet, these treatments often negatively affect ongoing quality of life, even for cured patients, by significantly compromising function and aesthetics. Patients with HNSCC with HPV-negative tumors, including those harboring *HRAS* mutations (5% of HNSCC; ref. 7), have a worse prognosis than those with HPV-positive cancers. More effective treatments with lower toxicities are desperately needed. A recent return to focusing on inhibiting RAS membrane localization in these tumors prompted initiation of this study.

HRAS is the most frequently mutated RAS isoform in HNSCC (12). Although it was unknown whether mutant HRAS activity is required for tumor maintenance in this tumor type, the observation that resistance to the EGFR inhibitor cetuximab administered to unselected patients with HNSCC was frequently accompanied by the appearance of oncogenic mutations in RAS proteins (13) contributed to the perception that HRAS mutant HNSCC would be a candidate for treatment with FTIs. Evaluating this possibility, a small phase I trial of the clinical candidate FTI tipifarnib was initiated in HRAS mutant patients with HNSCC. Preliminary reports indicated partial responses in a subset (55%) of 18 patients (14). However, because there are more than 50 other FTase substrates, whether the clinical response to FTI treatment can be attributed to HRAS inhibition remained to be resolved. In this study, we silenced HRAS expression and established that it is required for the growth and survival of HRAS mutant HNSCC cell lines. We also showed that treatment with the FTI tipifarnib at doses that blocked HRAS farnesylation and membrane association partially phenocopied genetic loss of HRAS. Using both candidate approaches and unbiased reverse-phase protein array (RPPA) pathway activation mapping, we demonstrated that both HRAS knockdown and FTI treatment could result in compensatory increases in ERK MAPK activity and cause reprogramming of prosurvival signaling pathways. We subsequently applied a CRISPR-Cas9 genetic screen to identify clinically relevant targets of drugs that could enhance sensitivity to tipifarnib. Among the top hits were components of both key RAS effector pathways, the RAF–MEK–ERK MAPK cascade and the PI3K–AKT–mTOR pathway. We found that, although HRAS mutant HNSCC lines were surprisingly insensitive to ERK1/2 inhibition alone, addition of either ERK1/2 or PI3K inhibitors enhanced sensitivity to tipifarnib. Finally, we observed that tipifarnib can upregulate markers of epithelial-to-mesenchymal transition (EMT), which can contribute to therapeutic resistance. That FTI-induced upregulation of EMT could be blocked by ERK inhibitor treatment suggested an additional basis for the efficacy of this combination. Our results indicate that these combinations warrant further investigation for the treatment of HRAS mutant HNSCC.

Materials and Methods

Further information can be found in the Supplementary Materials and Methods.

HNSCC cell lines and culture

HN30 (HRAS G12D, RRID:CVCL_5525) was a kind gift from Dr. Silvio Gutkind (University of California at San Diego). KYSE30 (HRAS Q61L, RRID:CVCL_1351) was acquired from the Tissue Culture Facility at the Lineberger Comprehensive Cancer Center, UNC-CH, Chapel Hill. UMSCC4 (HRAS G12V, RRID:CVCL_7751), UMSCC11a (HRAS WT, RRID:CVCL_7715), UMSCC43 (HRAS G12V, RRID:CVCL_7755), and UMSCC63 (HRAS G12D, RRID:CVCL_L130) were acquired from the University of Michigan, through a Materials Transfer Agreement. Cells were cultured in DMEM and/or Ham's F12 and penicillin/streptomycin under standard conditions at 37°C. Cell lines were STR-authenticated, regularly monitored for *Mycoplasma* infection using the MycoAlert *Mycoplasma* Detection Kit (Lonza), and used no longer than 3 months after thawing.

Lentivirus shRNA

shRNA constructs from The RNAi Consortium (TRC) targeting *HRAS* [TRC 40088, 40091, 10358] were cloned into pLKO.1 (RRID:Addgene_8453). Lentivirus particles were produced in HEK293T cells (RRID:CVCL_0063) using packaging plasmids DNA, pMD2.G (RRID:Addgene_12259) and psPAX2 (RRID:Addgene_12260) from Addgene (15). HNSCC cells were transduced with 0.5 mL of virus-containing supernatant in the presence of polybrene (8 μg/μL) and incubated overnight prior to selection in puromycin (5 μg/μL). Knockdown efficiency was confirmed by Western blot analysis.

Proliferation assays

Proliferation assays were performed as previously described and quantitated using MTT or alamarBlue (15).

Apoptosis and cell-cycle assays

Cells were subjected to 5 days of inhibitor treatment or HRAS knockdown. To detect apoptosis, treated cells were analyzed with the Annexin V-FITC Staining Kit (R&D Systems). For cell-cycle analysis, cells were fixed in 70% ethanol overnight and stained with propidium iodide (4 μg/mL) containing RNAse A (100 μg/mL). Flow cytometry was performed using a CytoFLEX S (Beckman Coulter).

Immunoblotting

Cell lysates were prepared in Laemmli buffer, and equal amounts of protein were subjected to SDS-PAGE, transferred to methanol-activated PVDF membranes, and probed with primary antibodies against the specific targets (largely 1:1,000 dilution), followed by appropriate secondary antibodies [anti-rabbit (NA934V) and anti-mouse (NA931V, RRID:AB_772210; GE Healthcare) at 1:10,000 dilution]. Proteins were detected by chemiluminescence (Amersham ECL Western Blotting Detection Kit, GE Life Sciences) and blots developed using the ChemiDoc MP Imaging System (BioRad, RRID:SCR_019037).

RPPA pathway activation mapping

Samples for RPPA analysis were prepared in four biological replicates (16). Briefly, cells were treated with inhibitor or DMSO vehicle control for the indicated times and lysed in T-PER tissue protein extraction reagent (Thermo Fisher Scientific). Protein quantity was normalized, lysates were suspended in 2× SDS sample buffer (Bio-Rad) supplemented with β-mercaptoethanol and boiled for 5 minutes, and stored at −80°C until arrayed. Lysates were printed on nitrocellulose-coated glass slides in four technical replicates and arrays were probed for target proteins. Biotin-labeled secondary antibodies, tyramine-based amplification system, and IRDye 680RD (LI-COR Biosciences) streptavidin fluorescence dye were used to amplify and detect the signal. Slides were scanned and signal intensity calculated using commercially available software (MicroVigene v5.1.0.0; VigeneTech, Inc. RRID:SCR_002820). Technical replicates (four per sample) were averaged, and the median taken across four experimental replicates. Results are reported as the fold-change of up- or downregulation of drug-

treated vs. vehicle-treated samples. Clustered heatmaps were generated using the pheatmap library in R 3.6.2 (RRID:SCR_016418).

CRISPR/cas9 loss-of-function genetic screens

A barcoded pooled CRISPR-Cas9 loss-of-function library consisting of 11950 gRNA against 2390 genes has been described previously (17). The pooled plasmid DNA was stock-amplified in Lucigen 10G Elite electrocompetent bacteria and cultured on LB agar plates to achieve 1 million colonies. After isolation, DNA was packaged in lentiviral particles generated using HEK293T cells. Titered viral particles were delivered to HN30 cells at a low multiplicity of infection (0.3). After puromycin selection, cells were treated with inhibitor or DMSO vehicle control for 2 or 4 weeks. Drug was refreshed every 3 to 4 days and cells were passaged upon reaching 80% confluency. Cells were maintained at 1,000× sequence coverage to prevent artificial selection pressure. Genomic DNA was extracted using Qiagen DNeasy Blood and Tissue Kit. Samples were prepared for sequencing by PCR amplification as described previously (18). Sequencing was performed on an Illumina NextSeq 500 with 75bp, single-end reads at a final concentration of 3 pmol DNA. DNA was loaded with a PhiX spike of greater than 20% to enhance signal complexity. The counts of each gRNA were analyzed to identify targets that sensitized or caused resistance to treatment.

TritonX-114 phase separation

Cells were treated with inhibitor for 24 hours, then subjected to phase separation by lysing in precondensed Triton X-114 solution (19). Lysates were separated twice into detergent and aqueous phases by incubating at 37°C, then prepared for Western blot by addition of 4× SDS buffer and boiling. Immunoblotting was performed to detect endogenous HRAS and the vinculin loading control.

Statistical analysis

Bliss synergy scores were calculated as described previously (20). All quantitative assays were done at least three times independently and data are represented as the mean ± SD. A two tailed *t* test was used to calculate *P* values; $P < 0.05$ was considered significant.

Data availability statement

The data generated in this study are available within the article and its supplementary data files.

Results

HRAS mutant HNSCC cell lines are dependent on HRAS for their proliferation and survival

To study the dependence of HNSCC cell lines on mutant HRAS, we used three different lentiviral shRNAs to knock down HRAS expression in a panel of five HRAS mutant HNSCC cell lines. Knockdown was confirmed by immunoblotting (**Fig. 1A**). Anchorage-dependent cell growth over a period of 10 days was evaluated by MTT assay (**Fig. 1B**). HRAS knockdown nearly ablated cell proliferation of all HRAS mutant lines tested. We next evaluated anchorage-independent growth over 2 weeks. HRAS depletion impaired proliferation in 3D Matrigel of HNSCC cell lines harboring mutant HRAS but not a cell line harboring wild-type (WT) HRAS (**Fig. 1C**; Supplementary Figs. S1A and S1B). HRAS depletion also dramatically impaired 2D clonogenic growth of HRAS mutant cells (**Fig. 1D**).

Next we wanted to determine whether HRAS depletion inhibits growth by causing growth arrest or cell death. We performed cell-cycle analysis using flow cytometry. Depletion of HRAS resulted in variable alterations in cell-cycle distribution (**Fig. 1E** and **F**; Supplementary Fig. S1C). We then determined, by Annexin-FITC staining, that the HRAS mutant cells were highly susceptible to induction of apoptosis upon HRAS knockdown (**Fig. 1G**; Supplementary Fig. S1D), whereas the HRAS WT cell line was not (Supplementary Figs. S1D and S1E). Together, these results indicate that mutant HRAS is important for the proliferation and survival of HRAS mutant HNSCC cells, and, as anticipated, supports mutant HRAS as a therapeutic target in HNSCC.

Treatment of HRAS mutant HNSCC with the FTI tipifarnib inhibits cell growth and induces apoptosis

To determine the ability of the FTI tipifarnib to inhibit HRAS farnesylation in HRAS mutant HNSCC, we used TritonX-114 phase separation to evaluate HRAS partitioning into detergent (farnesylated) versus aqueous (nonfarnesylated) phases. All five HRAS mutant cell lines were sensitive to low nanomolar FTIs, displaying both redistribution into the aqueous phase and slower electrophoretic mobility, indicating lack of prenylation, after as little as 24 hours of tipifarnib treatment (**Fig. 2A**). Farnesylation is a permanent modification and HRAS has a half-life of 20 to 24 hours (21). Thus, the differing degrees of distribution of endogenous HRAS into the aqueous phase upon FTI treatment likely indicate differential regulation of HRAS transcription and/or translation in each cell line, as the upper band represents only proteins newly synthesized in the presence of FTIs. We also observed a variable effect on HRAS protein abundance at higher concentrations of tipifarnib (**Fig. 2B**).

We next evaluated the effect of tipifarnib on cell growth. Cells were treated for 5 days and viability was measured. Like genetic depletion of HRAS, tipifarnib treatment also reduced cell viability, in a dose-dependent manner, albeit with differing sensitivities among the cell lines (**Fig. 2C** and **D**). These lines were also sensitive to tipifarnib-mediated inhibition of 2D clonogenic growth (**Fig. 2E**) and anchorage-independent growth in Matrigel (**Fig. 2F**). Overall, their sensitivity profile in response to tipifarnib was very similar to their response to HRAS depletion. Notably, KYSE30 was the least sensitive to tipifarnib in 3D Matrigel. This cell line has a copy-number amplification in EGFR (22), which could explain the lack of sensitivity to FTI treatment in the growth factor-rich environment. As with genetic depletion of HRAS, there was little consistent change in cell-cycle distribution upon 72 hours of FTIs (**Fig. 2G**). Thus, FTI treatment phenocopies *HRAS* genetic depletion with respect to growth inhibition in HRAS mutant HNSCC cells.

HRAS genetic depletion can cause upregulation of MAPK and AKT signaling pathways

The RAF–MEK–ERK MAP kinase cascade and the PI3K–AKT–mTOR pathways are critical downstream effectors of RAS signaling (1), yet *KRAS* knockdown in a panel of KRAS mutant pancreatic ductal adenocarcinoma (PDAC) cell lines did not result in consistent loss of either pERK or pAKT (23). We observed that stable depletion of HRAS by lentiviral shRNA resulted in increased pERK and pAKT in a subset of HRAS mutant HNSCC lines (**Fig. 3A**).

Tipifarnib treatment partially phenocopies HRAS genetic depletion, causing compensatory increases in both ERK MAPK and AKT signaling

During the original development of FTIs more than 20 years ago, many studies were performed to assess their effects on cellular phenotypes such as morphology, proliferation, survival, cell-cycle progression, and tumorigenicity. With the advent of more modern technologies to address cell signaling in a higher throughput manner, it

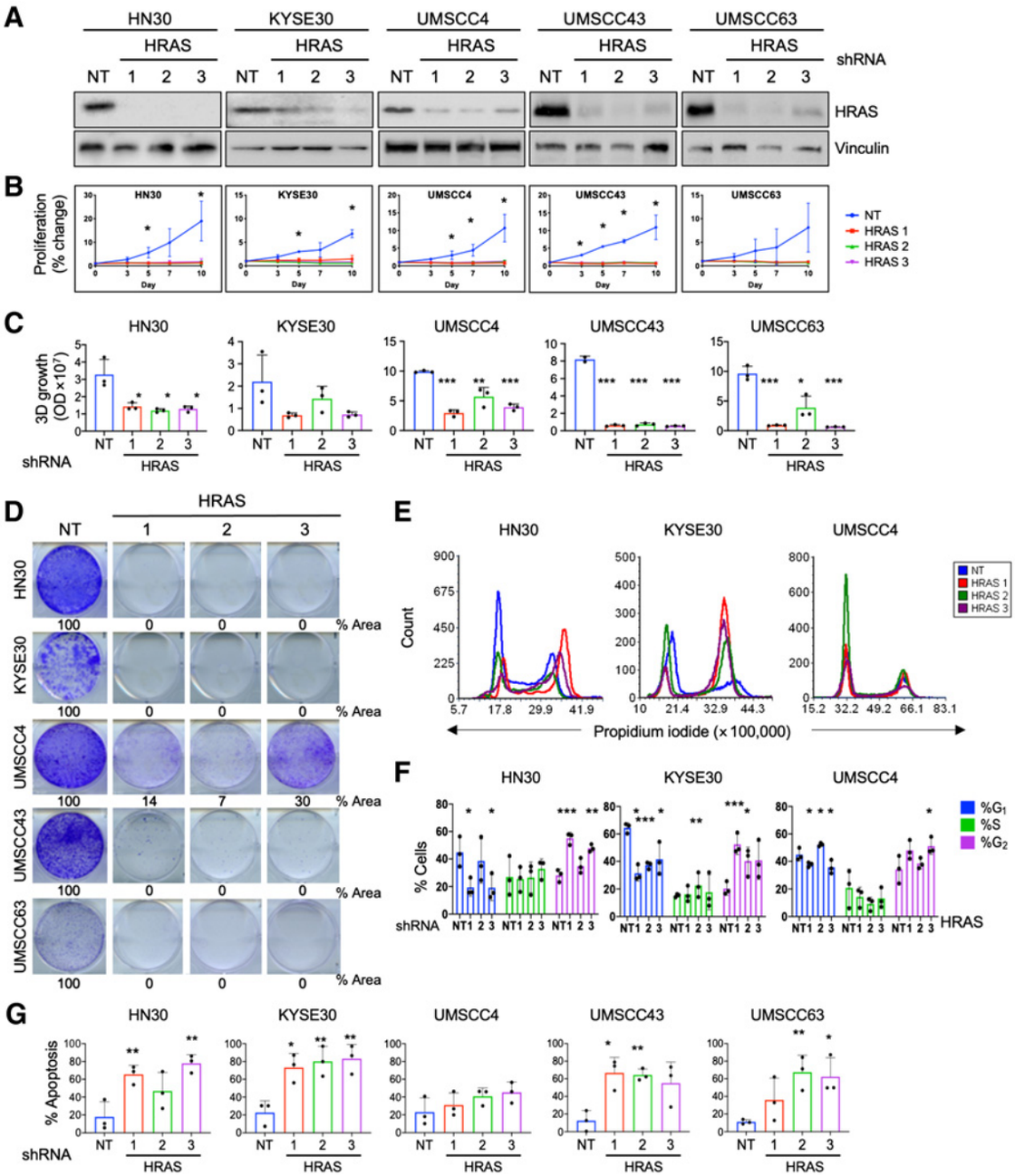

Figure 1.

HRAS mutant HNSCC cell lines depend on HRAS for their growth and survival. **A,** Western blots showing knockdown of HRAS protein. HRAS mutant HNSCC cell lines were transduced with anti-HRAS or nontargeting (NT) control shRNA and selected in puromycin for 72 hours. **B,** Anchorage-dependent 2D proliferation assay following HRAS knockdown. Cells were seeded in triplicate in 12-well plates and viability evaluated by MTT after 10 days. Data represent average ± SD of three biological replicates. *P* values are averages of the individual *P* value of each shHRAS compared with shNT for each time point (*, $P < 0.05$). **C,** Quantification of anchorage-independent 3D colonies formed after HRAS knockdown. Cells were grown in Matrigel for 2 weeks, then stained with alamarBlue. *P* values as in **B** (*, $P < 0.05$; **, $P < 0.01$; ***, $P < 0.001$). **D,** Representative 2D clonogenic assays showing colony formation after HRAS knockdown. Cells were plated in 6-well plates after lentiviral shRNA transduction and puromycin selection. After 10 days, colonies were stained with crystal violet. **E,** Histograms showing cell cycle distribution after HRAS knockdown. After 72 hours of shRNA transduction and selection, cells were stained with propidium iodide and subjected to flow cytometry. **F,** Quantification of data shown in **E**. Data represent average ± SD of three biological replicates. *P* values are averages of the individual *P* value of each shHRAS compared with shNT (*, $P < 0.05$; **, $P < 0.01$; ***, $P < 0.001$). **G,** Quantification of apoptosis after HRAS knockdown. After 5 days, cells were stained with Annexin V-FITC and propidium iodide and quantified by flow cytometry. Data represent average ± SD of three biological replicates. *P* values as in **F**.

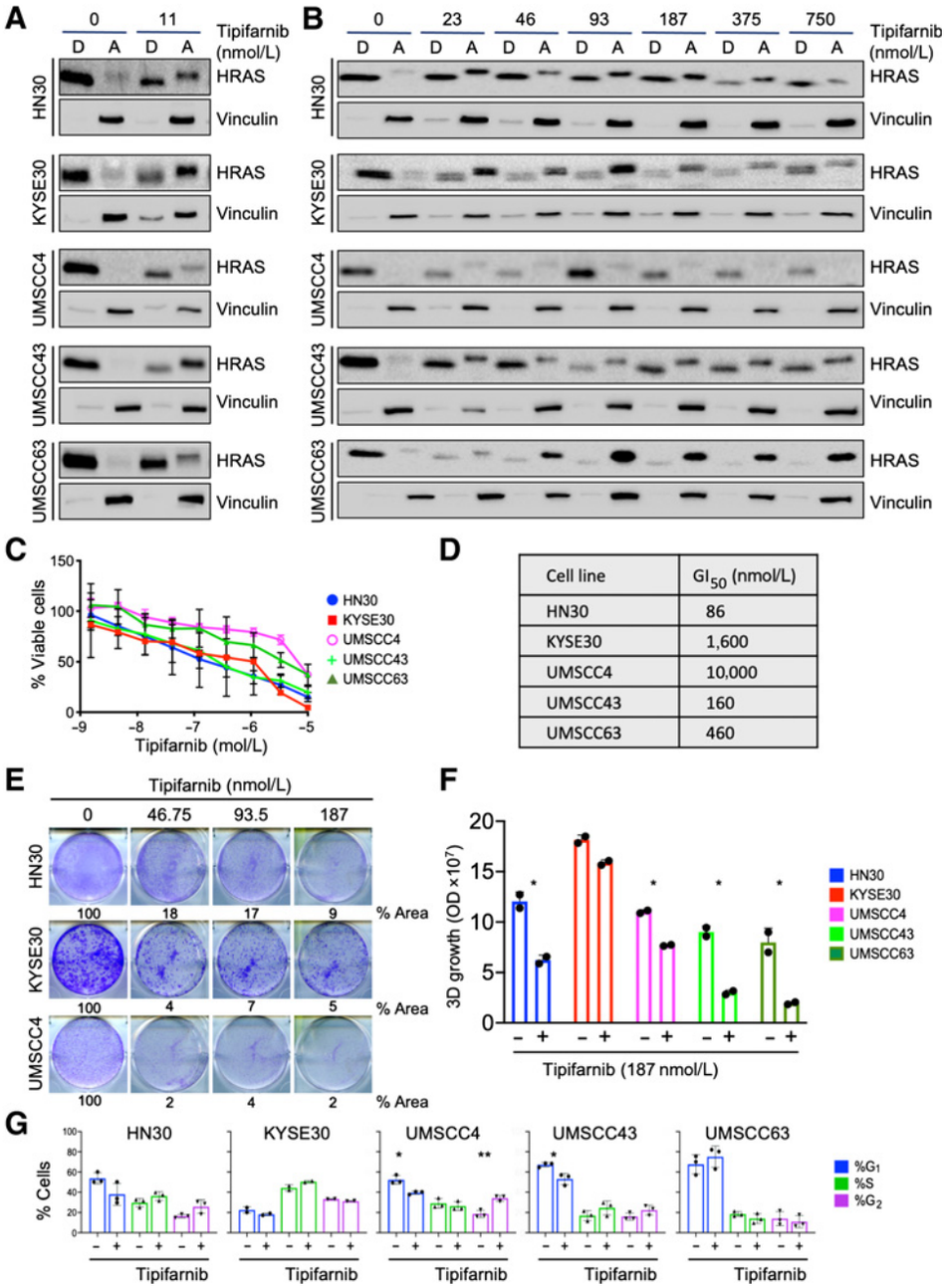

Figure 2.

FTI treatment phenocopies HRAS knockdown and inhibits growth of HRAS mutant HNSCC. **A,** Western blot showing distribution of HRAS into detergent ("D", membrane) and aqueous ("A", cytosol) phases. Indicated HRAS mutant cells were treated with FTI tipifarnib or DMSO vehicle control for 24 hours and subjected to TritonX-114 phase separation. Nonfarnesylated proteins migrate more slowly (top bands) than farnesylated proteins (bottom bands). **B,** Western blot analysis showing variable changes in HRAS abundance upon tipifarnib treatment. Cells treated as in **A**. **C,** AlamarBlue assay quantifying cell viability after tipifarnib treatment for 5 days. Data are average ± SD of three biological replicates. **D,** GI_{50} of tipifarnib in HRAS mutant HNSCC cell lines in **C**. **E,** Representative 2D clonogenic assay showing quantified growth inhibition (% plate area covered by cells) after treatment with tipifarnib for 10 days. **F,** Quantification of 3D colonies formed in Matrigel after treatment with tipifarnib (187 nmol/L). Data are average of two technical replicates. *P* value: treatment versus DMSO control (*, $P < 0.05$). **G,** Quantification of cell-cycle distribution after treatment with tipifarnib. Data are average ± SD of three biological replicates. *P* value: treatment versus DMSO control (*, $P < 0.05$; **, $P < 0.01$).

has now become possible to more thoroughly examine the signaling changes that occur when farnesylation is blocked. To understand the signaling changes conferred by tipifarnib treatment in HRAS mutant HNSCC cells, we performed unbiased RPPA pathway activation mapping (16). We treated three cell lines (HN30, KYS30, and UMSCC4) with FTIs for 24 or 48 hours and prepared lysates for analysis of ∼200 phosphorylated and total proteins. RPPA pathway activation mapping revealed an increase in pERK1/2 and pAKT at both time points following FTI treatment (**Fig. 3B**). Tipifarnib-mediated compensatory increases in pERK have also been observed in HRAS mutant thyroid cancer cells (24). In addition, several other RAS signaling-associated kinases and transcription factors were upregulated, including PAK1, p38 (*MAPK14*), NF-κB, and ATF2. Conversely, we observed decreases in several receptor tyrosine kinases such as EGFR, c-Kit, and MET, and targets of the mTOR pathway such as p70 ribosomal protein S6 kinase (S6K). We noted a modest increase of inhibitory phosphorylation of the anti-apoptotic protein BCL2, suggesting an early attempt by the cell to counter the stress of shutting down multiple pathways by inducing apoptosis.

Tipifarnib treatment inhibits RHEB farnesylation but not mTOR signaling

The spectrum of biological activities of farnesylated proteins (25–27) has greatly complicated our ability to understand the mechanistic consequences of inhibiting farnesyltransferase. Other farnesylated proteins include RAS-related small GTPases such as RHEB, a key

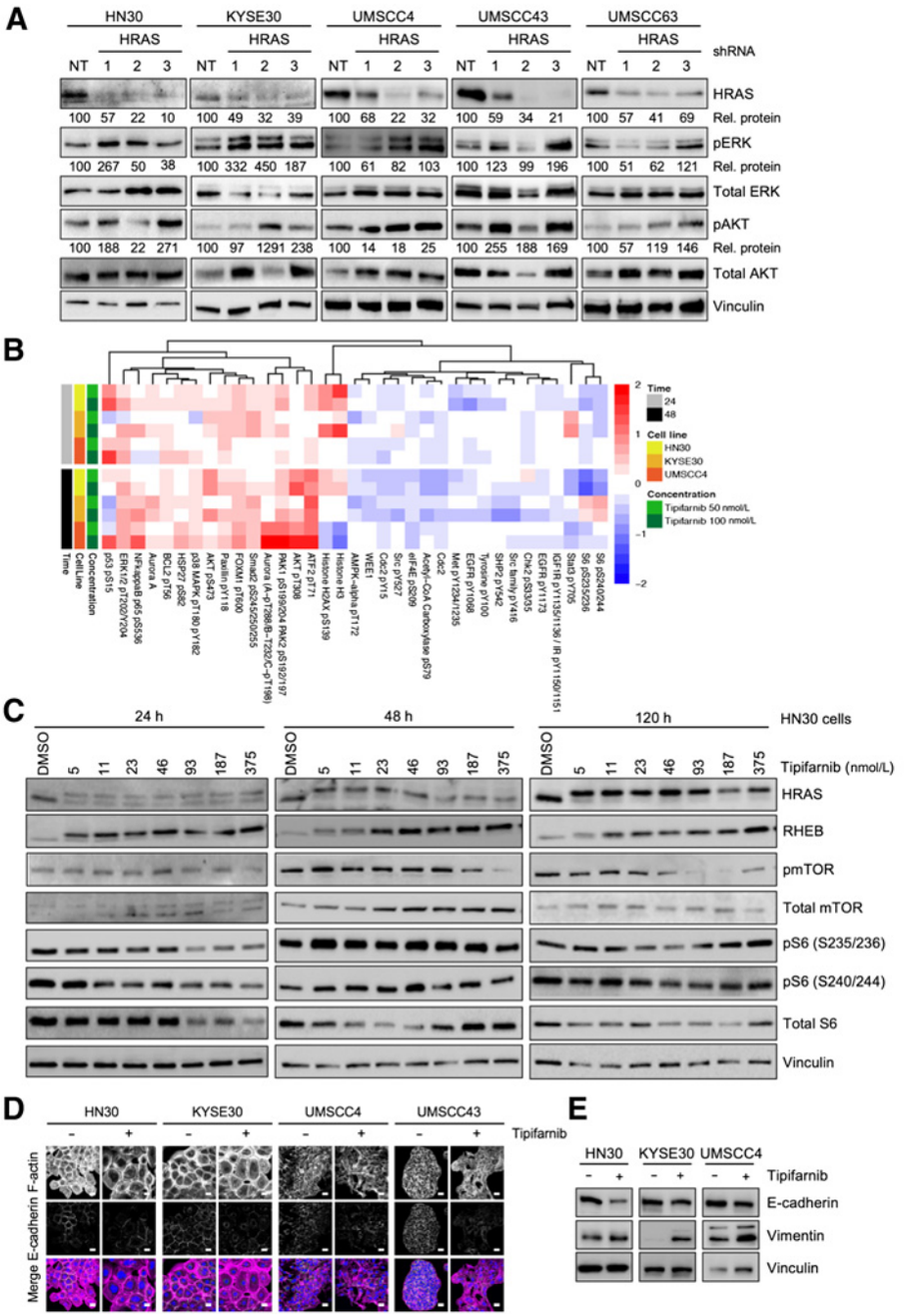

Figure 3.

HRAS depletion and tipifarnib treatment can cause compensatory upregulation of ERK MAPK and AKT signaling pathways; induction of morphological changes. **A,** Western blot analysis showing increased levels of pERK1/2 and pAKT in some cell lines after HRAS knockdown. Cells were transduced with three different anti-HRAS shRNAs or NT control and selected in puromycin for 72 hours prior to blotting for phosphorylated and total ERK and AKT. Densitometry was used to quantitate ratios of phosphorylated to total proteins ("Rel. proteins"), normalized to NT control. **B,** Heatmap showing the top 35 differentially regulated proteins or phosphoproteins in the indicated cells treated with tipifarnib or DMSO vehicle for 24 or 48 hours. Cell lysates were subjected to RPPA analysis. Red: increase; blue: decrease. **C,** Western blots of HN30 cells showing signaling downstream of HRAS and RHEB after 24, 48, or 120 hours of treatment with tipifarnib at the indicated concentrations. **D,** Immunofluorescence images showing expression and distribution of F-actin and E-cadherin in cells treated with tipifarnib (200 nmol/L) or DMSO vehicle. In the merge image, F-actin is shown in magenta, E-cadherin in green, and the nucleus in blue. Scale bar = 20 μm. **E,** Western blots showing expression of E-cadherin and vimentin after treatment as in **D**.

regulator of mTOR signaling. RHEB must be farnesylated to promote S6 kinase activation through mTOR, and has been suggested to promote RAS-independent consequences of FTIs (28, 29). Therefore, we investigated the effect of tipifarnib treatment on RHEB farnesylation and mTOR signaling in HNSCC. Tipifarnib induced complete loss of farnesylation as indicated by gel shift (**Fig. 3C**), accompanied by a possible attempt at compensation by upregulating RHEB expression (**Fig. 3C**). However, despite the robust inhibition of RHEB processing at 24 hours at the lowest dose of FTIs, we did not observe a direct effect on activity of mTOR as measured by its own phosphorylation status. Phosphorylation of mTOR did decrease upon long-term treatment at higher concentrations. We also observed a variable decrease in the activity of mTOR substrates S6K and S6 at 24 and 48 hours (**Fig. 3B** and **C**); however, this was restored over long-term treatment, perhaps due to compensatory activation of ERK and/or AKT. Thus, tipifarnib-mediated loss of RHEB farnesylation is insufficient to prevent activation of mTOR in HRAS mutant HNSCC.

Tipifarnib induces morphologic changes and EMT

Some of the earliest recognized effects of FTIs included alterations in actin-mediated cell morphology (30–32). Such alterations can reflect changes in epithelial-to-mesenchymal transition (EMT) status. However, this had not been investigated in HNSCC. We therefore applied confocal immunofluorescence microscopy to investigate cell

morphology and the F-actin cytoskeleton in the HRAS mutant HNSCC cell lines. We observed remarkable heterogeneity in cell morphology and F-actin structures, in both treated and untreated conditions (**Fig. 3D**). For instance, whereas KYSE30 cells are round and have significant cortical actin, UMSCC4 cells are smaller and have a fibroblast-like morphology with F-actin stress fibers. In line with these observations, we also observed heterogeneity in basal EMT status based on immunoblotting for the epithelial marker E-cadherin and the mesenchymal marker vimentin (Supplementary Figs. S2A and S2B). KYSE30 cells are characterized by high E-cadherin levels and hardly any vimentin, indicative of a more epithelial-like basal state, in line with the observed cell morphology. In contrast, UMSCC4 cells have significantly higher vimentin than E-cadherin levels, indicating a more mesenchymal-like basal state, also in line with their morphology. Together, both the imaging and the Western blot studies indicate that all the HNSCC lines are in a partial EMT state under basal conditions. Imaging studies showed that tipifarnib increased cell size and decreased E-cadherin expression (**Fig. 3D**), which was confirmed by Western blot analysis (**Fig. 3E**). Conversely, the mesenchymal marker vimentin was increased upon tipifarnib treatment (**Fig. 3E**), in contrast to early findings in RAS-transformed fibroblast model systems, which reverted to a more flattened epithelial-like morphology upon treatment with FTIs (30, 31). These data indicate that tipifarnib treatment can induce EMT in HRAS mutant HNSCC, regardless of their relative sensitivity to tipifarnib-mediated growth suppression. EMT is associated with resistance and poor treatment outcome in cancers treated with conventional cytotoxic therapies (33, 34). We hypothesize that induction of EMT could similarly cause emergence of resistance in tipifarnib treated HNSCC tumors.

CRISPR/cas9 loss-of-function genetic screen identifies both expected and novel targets for sensitization of HRAS mutant HNSCC to tipifarnib

Acquired treatment resistance is a challenge for all targeted cancer therapies. Forecasting the potential mechanisms of resistance and improving sensitization to existing therapies is crucial for successful cancer treatment. We used lentiviral transduction to deliver a barcoded CRISPR/Cas9 druggable genome library, targeting ~2,500 genes with five guide RNAs each (17), to tipifarnib-treated HRAS mutant HNSCC HN30 cells. Following puromycin selection, cells were treated for 2 or 4 weeks at 1,000× library coverage with tipifarnib at the GI_{25}, a dose that caused some inhibition of FTase without substantially inhibiting cell growth. Surviving cells were pooled and sequenced to identify enriched or depleted sgRNAs (see counts in Supplementary Tables S1 and S2). The sgRNA counts were entered in HitSelect, a published algorithm (35), to calculate rank and effect size. We compared the top 10% of genes from each time point, using stringent criteria of at least three active sgRNAs of the five total for each gene. At the 2-week time point, the top hit (**Fig. 4A**) was *FDPS*, encoding farnesyl diphosphate synthase, which catalyzes the production of farnesyl isoprenoids. Loss of *FDPS* enhanced cell sensitivity to the FTI tipifarnib, consistent with impaired synthesis of the isoprenoids required for farnesylation. Other top hits included regulators of PI3K–AKT–mTOR signaling (*RAC1, PIK3R1/2, AKT2, RPTOR*) and regulators of metabolism (*RPTOR, ULK1, PFKL, CPT1A;* **Fig. 4A** and **B**). *IQGAP2*, which interacts with RAC1 and RHO GTPases (36) and inhibits EMT (37) was the top hit at the 4-week time point, consistent with the possibility that tipifarnib induction of EMT may limit its efficacy in HRAS mutant HNSCC. Other top hits included positive regulators of RTK-RAS signaling (*ERBB3, SOS2, HRAS*, and *NRAS*) and protein translation (*RPS6KA3*; **Fig. 4C** and **D**). Conversely to the depletion of the above genes, we also observed enrichment of the RASGAP *NF1* and tumor suppressor *NF2*, encoding MERLIN (**Fig. 4D**). These inhibit RAS signaling and their loss has been linked to resistance to tipifarnib in HRAS mutant thyroid cancer models (24).

At the 4-week time point, another top hit was *CXCR4*, a GPCR receptor for the CXCL12 ligand, also known as SDF-1, that drives metastasis homing. CXCL12/CXCR4 signaling exerts its effects through a plethora of RAS- and RHO-mediated pathways (38). Overexpression of either component has been identified as a potential biomarker for tipifarnib activity in blood cancers (39). The serine/threonine kinase ULK1, which initiates autophagy, was a top sensitizer to tipifarnib in the CRISPR screens at both time points. We also performed KEGG pathway enrichment analysis for the top 10% of hits from each dataset (Supplementary Fig. S3A). Prominent among these were genes regulating metabolic pathways, indicating that metabolic reprogramming is an important component of the response to tipifarnib. We and others have shown that MAPK inhibition sensitizes KRAS mutant PDAC to autophagy inhibition (40, 41) and here we observed that tipifarnib can upregulate compensatory MAPK signaling in HRAS mutant HNSCC. To begin to validate these interesting hits, we performed preliminary experiments by treating HRAS-mutant HNSCC cells with a combination of tipifarnib and either the autophagy inhibitor chloroquine or the CXCR4 inhibitor WZ811. In a subset of cell lines, these combinations were synergistic, as indicated by Bliss scores less than one (Supplementary Figs. S3B and S3C). Interestingly, T-cell receptor signaling was also prominent, supporting the idea that FTIs could be combined with immunotherapy for improved clinical benefit in HRAS mutant HNSCC. These screens identify potential combinations that warrant further investigation in future studies.

Combination of the FTI tipifarnib with ERKi, PI3Ki, or mTORi causes apoptosis in HRAS mutant HNSCC

Both RPPA (**Fig. 3B**) and KEGG pathway analysis (Supplementary Fig. S3A) also confirmed that many hits in our screen regulate the ERK MAPK and PI3K–AKT–mTOR pathways. We first selected the ERK1/2-selective inhibitor SCH772984 and the PI3K alpha-selective inhibitor alpelisib for further investigation. Cells were treated for 5 days with the combinations of tipifarnib with a dose–response matrix of each inhibitor at doses that partially or completely inhibited their respective targets (**Fig. 4E** and **F**). Cell viability was quantified by alamarBlue, and the GI_{50} (**Fig. 4G** and **H**) and Bliss synergy scores were calculated (**Fig. 4I** and **J**). Both inhibitors sensitized cells to tipifarnib and enhanced the growth inhibition induced by either single agent alone (**Fig. 4G** and **H**; Supplementary Fig. S3D), with GI_{50}s that were many-fold lower than the doses required to inhibit signaling.

To determine whether these combinations were simply cytostatic or could also induce cell death, we treated cells with tipifarnib in combination with a range of concentrations of PI3K-alpha inhibitor or ERK inhibitor that caused complete to partial inhibition of their respective targets (**Fig. 4E** and **F**). Treatment with single agents caused a modest amount of apoptosis which trended higher upon combination treatment (**Fig. 5A–D**). Some lines were sensitive to both combinations, whereas others were sensitive to only one. For example, HN30 and UMSCC63 were sensitive to FTI + ERKi and FTI + PI3Ki. KYSE30 was sensitive to FTI + ERKi whereas UMSCC43 was sensitive only to FTI + PI3Ki, and only at higher doses. Sensitivity to the combinations generally correlated to sensitivity to the individual

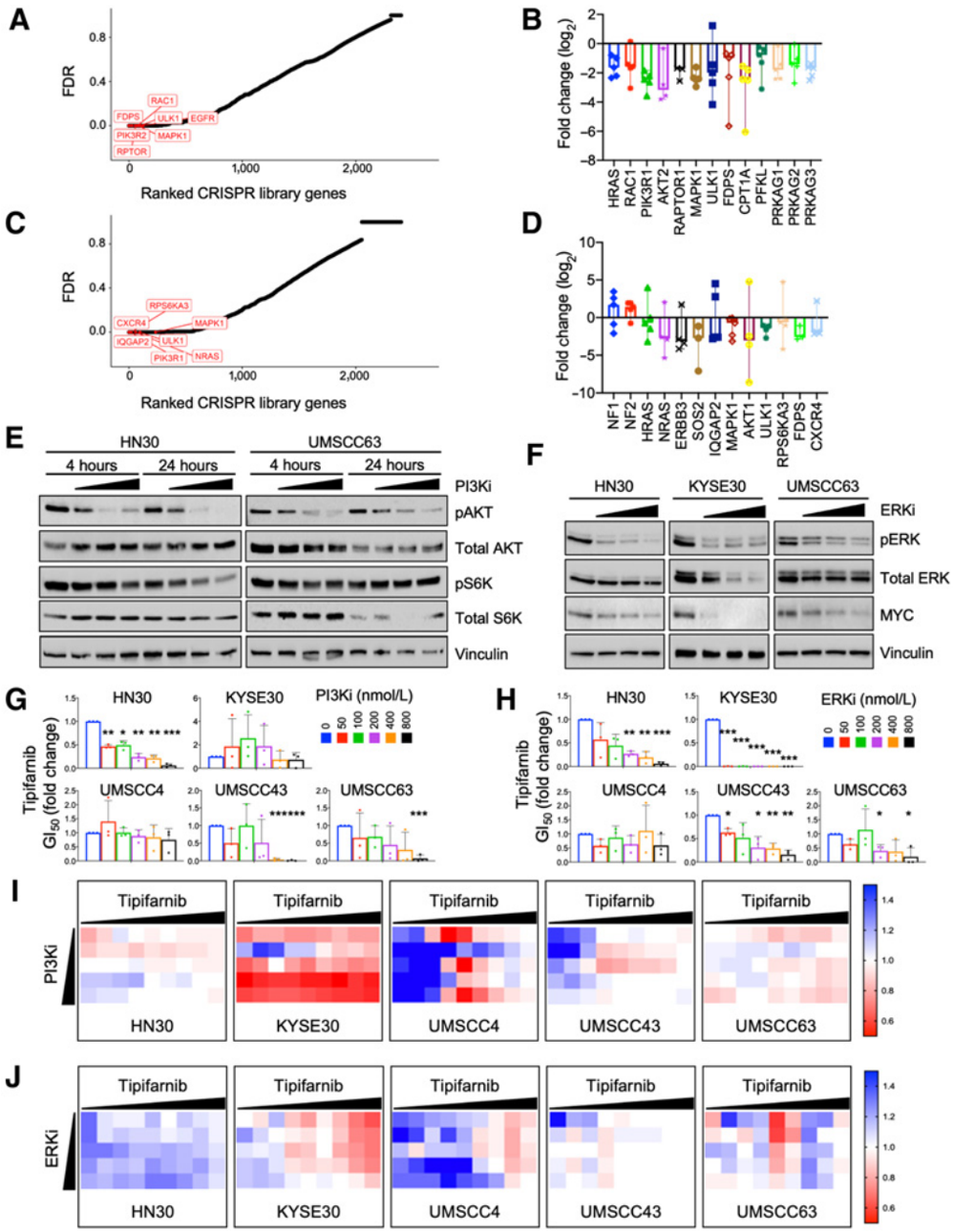

Figure 4.

CRISPR-Cas9 loss-of-function (LOF) screen identifies known and novel targets to sensitize cells to tipifarnib treatment. **A,** FDR for each gene in the CRISPR library at the 2-week time point. Top hits are highlighted in red. **B,** Fold change of gRNA against indicated genes in the library after 2 weeks of treatment. Data represented as median with range. **C,** FDR for each gene in the CRISPR library at the 4-week time point. Top hits are highlighted in red. **D,** Fold change for gRNA against indicated genes in the library after 4 weeks of treatment. Data represented as median with range. **E,** Western blot analysis showing target inhibition of PI3K signaling pathway by PI3K-alpha inhibitor alpelisib. Cells were treated for 4 or 24 hours at 100, 200, and 400 nmol/L. **F,** Western blot analysis showing target inhibition of ERK MAPK pathway by ERK1/2 inhibitor SCH772984. Cells were treated for 48 hours at 100, 200, and 400 nmol/L. **G,** Fold change in tipifarnib GI_{50} when combined with indicated concentrations of PI3K-alpha inhibitor alpelisib. *P* values: combination versus tipifarnib alone (*, $P < 0.05$; **, $P < 0.01$; ***, $P < 0.001$). **H,** Fold change in tipifarnib GI_{50} when combined with indicated concentrations of ERK1/2 inhibitor SCH772984. *P* values: combination versus tipifarnib alone (*, $P < 0.05$; **, $P < 0.01$; ***, $P < 0.001$). **I,** Bliss scores quantifying synergy between tipifarnib (1.5 nmol/L–10 μmol/L) and PI3K-alpha inhibitor (50–800 nmol/L). **J,** Bliss scores quantifying synergy between tipifarnib (1.5 nmol/L–10 μmol/L) and ERK1/2 inhibitor (50–800 nmol/L).

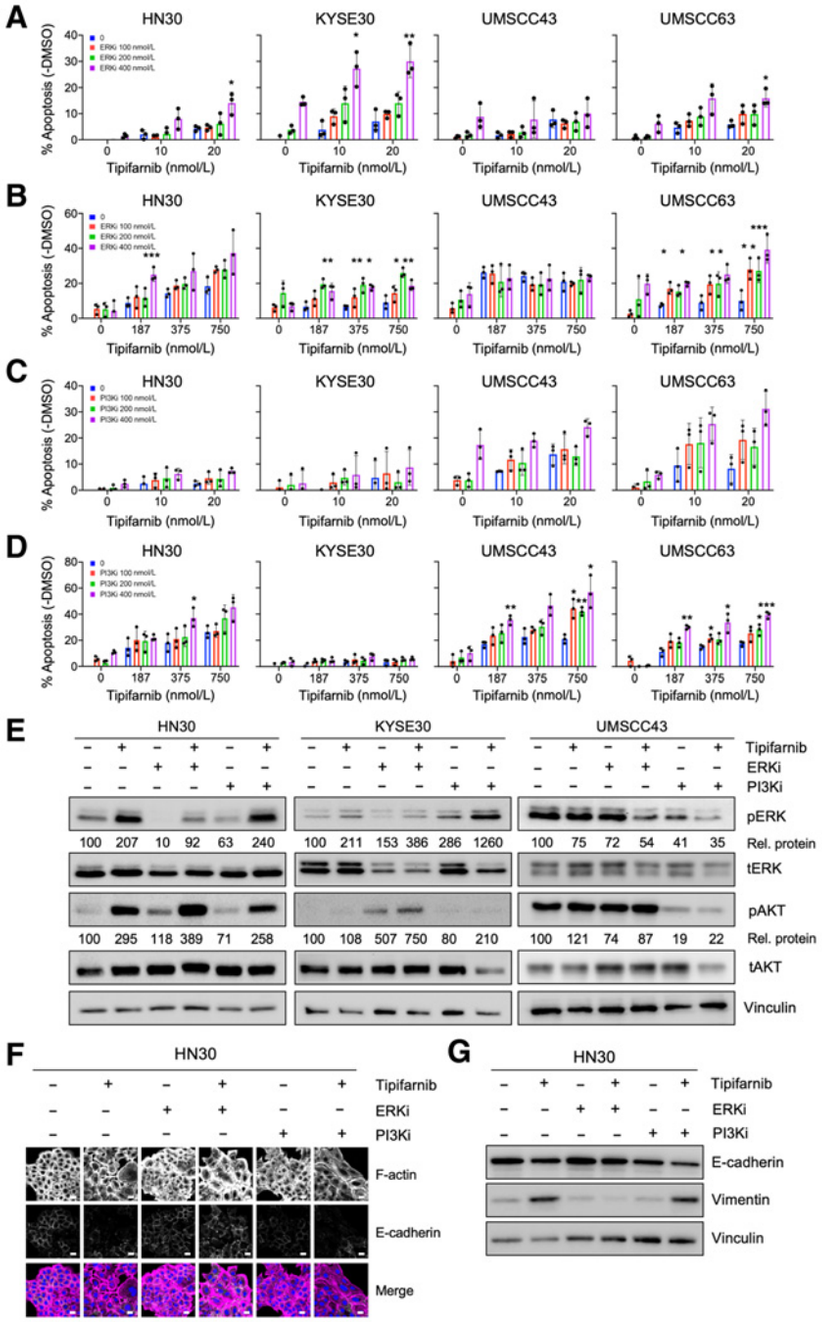

Figure 5.

Combination of FTI tipifarnib with ERKi or PI3Ki enhances apoptosis and induces EMT in HRAS mutant HNSCC. **A–D,** Quantification of apoptosis in cells treated with low (10–20 nmol/L, **A** and **C**) or high doses (187–750 nmol/L, **B** and **D**) of tipifarnib and 100–400 nmol/L of ERKi (SCH772984) or PI3Ki (alpelisib) for 5 days. Annexin-FITC positive cells were quantified and negative control DMSO values were subtracted. Data represent average ± SD of three independent replicates. *P* value: combination versus tipifarnib alone (*, $P < 0.05$; **, $P < 0.01$; ***, $P < 0.001$). **E,** Western blots showing target inhibition of ERK1/2 and AKT. Cells were treated for 24 hours with tipifarnib (200 nmol/L) and ERKi (400 nmol/L) or PI3Ki (400 nmol/L) in cell lines displaying differential sensitivity profiles to the combinations. Densitometry was used to quantitate ratios of phosphorylated to total proteins ("Rel. proteins"), normalized to DMSO control. **F,** Immunofluorescence images showing expression and distribution of F-actin and E-cadherin in response to the combinations or drugs alone, treated as in **E**. In the merge image, F-actin is shown in magenta, E-cadherin in green, and the nucleus in blue. Scale bar = 20 μm. **G,** Western blots showing expression of E-cadherin and vimentin in response to the combinations or drugs alone, treated as in **E**.

agents. Bliss scores indicated synergy to both or either of the inhibitors (Supplementary Figs. S4A–S4D).

In agreement with the genetic sensitizer screen, RPPA analysis also showed that FTI treatment causes upregulation of MAPK/ERK and PI3K/AKT pathway signatures (Supplementary Figs. S4E and S4F). We sought to analyze the signaling changes in these pathways upon combination treatments in three different cell lines with differential sensitivity to these inhibitors. We observed a compensatory increase in phosphorylation of AKT and ERK1/2 in cell lines insensitive to the combinations of FTI/PI3Ki (KYSE30) and FTI/ERKi (UMSCC43), respectively (**Fig. 5E**), possibly explaining their insensitivity to these particular combinations.

To evaluate whether combining tipifarnib with ERKi or PI3Ki would rescue the EMT induced by tipifarnib alone, we analyzed the expression of E-cadherin and vimentin by immunofluorescence imaging and Western blotting. Tipifarnib alone, PI3K inhibitor alone, or the combination decreased E-cadherin and increased vimentin, indicating an EMT (**Fig. 5F** and **G**; Supplementary Figs. S5A–S5D). In contrast, ERK inhibitor alone or the combination maintained E-cadherin levels and prevented the increase in vimentin expression induced by tipifarnib alone. This indicates the reverse of EMT (i.e., MET). These results show that the combination of FTIs with ERK inhibition may be superior to a single agent and could prevent or ameliorate emergence of resistance due to EMT. To extend this result, in addition to the

ERK1/2-selective inhibitor SCH772984, we also determined that tipifarnib synergistically enhanced apoptosis when combined with BVD-523/ulixertinib, a clinical candidate ERK inhibitor (Supplementary Figs. S6A–S6C).

Finally, we sought to identify a combination that could overcome the resistance of UMSCC4 to tipifarnib with or without PI3Ki or ERKi (**Fig. 6A** and **B**). RPPA analysis showed that, uniquely in UMSCC4 cells, FTI increased activation of p70 S6K and phosphorylation of its substrate BAD at the inhibitory site S136 (**Fig. 6C**), which decreases pro-apoptotic BAD activity and promotes cell survival. As p70 S6K is a direct substrate of mTOR, we speculated that blocking S6 activation using the mTOR inhibitor rapamycin could overcome this survival-

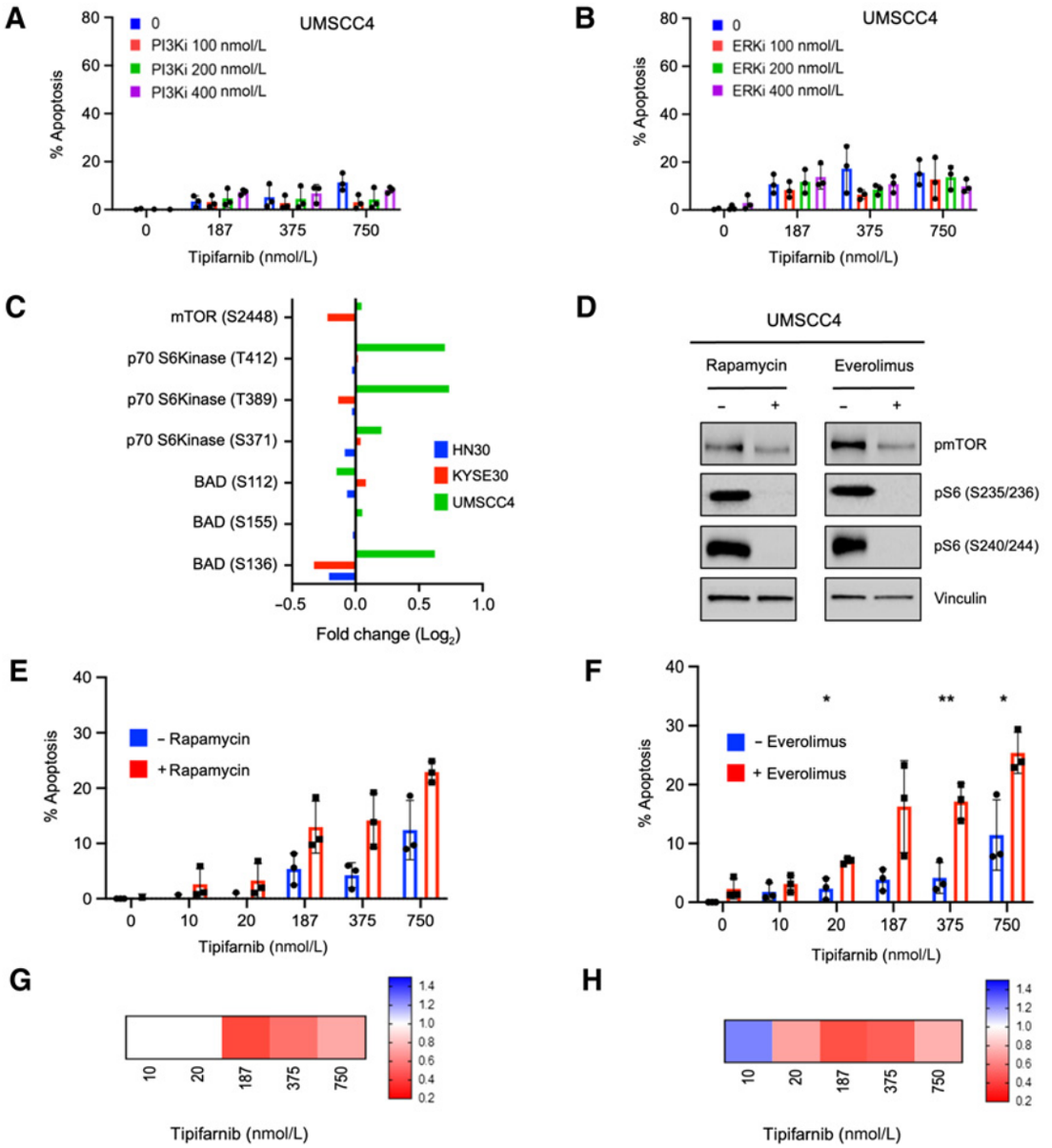

Figure 6.

Inhibition of mTOR/S6 activity is critical to cause cell death in response to tipifarnib treatment of refractory cells. **A** and **B,** Quantification of apoptosis in tipifarnib-refractory UMSCC4 cells. Cells were treated for 5 days with the indicated doses of tipifarnib and (**A**) the PI3K-alpha-selective inhibitor alpelisib or (**B**) the ERK1/2-selective inhibitor, SCH772984. Annexin-FITC positive cells were quantified and normalized to control. Data represent the average of three independent replicates; values above zero are shown. **C,** Fold change in mTOR and mTOR-regulated signaling showing increases in activity only in tipifarnib-refractory cells. Indicated cell lines were treated with tipifarnib and subjected to RPPA analysis as in **Fig. 3B**. **D,** Western blot analysis showing target inhibition of mTOR signaling. UMSCC4 cells were treated with mTORCi rapamycin (15 nmol/L) or everolimus (25 nmol/L) for 24 hours. **E** and **F,** Apoptosis assays showing increased efficacy of tipifarnib in refractory cells in the presence of mTORCi. UMSCC4 cells were treated with tipifarnib alone or in combination with rapamycin or everolimus. Data represent the average ± SD of three independent replicates (*, $P < 0.05$; **, $P < 0.01$; ***, $P < 0.001$). **G** and **H,** Bliss scores quantifying synergy between tipifarnib (10–750 nmol/L) and mTOR inhibitors rapamycin (15 nmol/L) and everolimus (25 nmol/L).

promoting consequence of FTI treatment in UMSCC4 cells. We found that rapamycin or another clinical analog, everolimus, effectively shut down the activity of mTOR and p70 S6K (**Fig. 6D**), and the combination of tipifarnib with either agent increased apoptosis compared with single agent alone (**Fig. 6E** and **F**). The synergy of these combinations was shown by Bliss scores of less than one (**Fig. 6G** and **H**).

Discussion

On the basis of promising results from an initial phase I clinical trial in HNSCC, the farnesyl transferase inhibitor tipifarnib is currently in directed phase II clinical trials for the treatment of recurrent or metastatic HRAS mutant HNSCC (NCT02383927, NCT03719690) and was recently given fast track designation by the FDA for review. Although HRAS mutation is currently the key selection criterion for trial enrollment, the role of mutant HRAS as an independent driver of HNSCC growth was unknown. Previous reports had focused on its possible role in the context of HNSCC resistance to EGFR inhibitors erlotinib and cetuximab (42, 43). Our direct demonstration that mutant HRAS protein is required for the growth and survival of HNSCC firmly credentials it as a therapeutic target in this disease. In agreement, a study published while this article was in preparation showed that only HRAS mutant, but not HRAS WT, HNSCC cell lines, and PDX models were susceptible to growth inhibition *in vitro* and *in vivo* by tipifarnib (44). However, although we have shown here that tipifarnib is fully capable of blocking HRAS farnesylation, membrane association, and signaling in HNSCC, it is not clear that inhibition of HRAS alone is sufficient to explain tipifarnib efficacy. Neither HRAS mutation nor dependence is fully predictive of tipifarnib response. This should not be surprising, considering that FTIs are not anti-RAS drugs, but rather are highly selective inhibitors of FTase, which has numerous farnesylated substrates (26, 27).

Our panel of HRAS mutant HNSCC cell lines represented the anatomic and histologic diversity of the head and neck region. We observed remarkable heterogeneity in basal morphology as well as response to tipifarnib treatment. Through unbiased pathway activation mapping and genetic screens, we found that the signaling changes induced by tipifarnib included compensatory upregulation of MAPK and PI3K–AKT, the two most prominent RAS effector pathways. Upregulation of these pathways has recently also been identified in tipifarnib-treated thyroid cancer models (24) but not bladder carcinoma (45) or HNSCC (44). We suspect that differences in experimental conditions explain the latter. Our work indicates that combining tipifarnib with inhibitors of these pathways is a logical next step. Patients are typically treated with the maximum tolerated dose of targeted therapies. Our data suggest that partial inhibition of two targets simultaneously could be therapeutically advantageous and may help in reducing drug-associated toxicities.

Likewise, our genetic loss-of-function screen also indicated that inhibitors of the MAPK and PI3K–AKT pathways should sensitize these tumors to FTIs. We validated these combinations and established that sensitivity to a particular combination correlated with lack of compensation by the alternative pathway. Previous reports from RAS-transformed fibroblasts and thyroid cancers support greater efficacy of the combination of FTIs with MEK or PI3K inhibitor as more effective than FTIs alone (24, 46). We observed that tipifarnib induced an ERK-mediated signaling signature, which led us to co-target the terminal node of the MAPK signaling pathway. HRAS promotes EMT in an ERK-dependent manner (47). In turn, EMT promotes chemoresistance (33, 34). On the basis of our finding that tipifarnib induces EMT in HRAS mutant HNSCC despite inhibiting HRAS itself, and that combining tipifarnib with ERK inhibition but not PI3K inhibition prevents this induction, we propose that future trials preferentially assess this combination specifically in HRAS mutant HNSCC.

It will also be interesting to further validate other hits from our genetic sensitizer screen. Some, such as CXCR4 or ULK1, already have inhibitors under development or in the pipeline for clinical trials and are potentially actionable; others, such as IQGAP2, are more useful to further explore mechanisms of FTI sensitivity and resistance. In addition, it will be of great interest to further examine our preliminary data indicating that the mTOR inhibitors rapamycin and everolimus can overcome tipifarnib-driven inhibition of the pro-apoptotic protein BAD, thereby promoting apoptosis. Clinical trials have shown that everolimus lacks activity as monotherapy or in combination with cisplatin and cetuximab in unselected patients with HNSCC. However, a recent abstract presentation on a small phase II trial (NCT01111058) reported that patients with HNSCC with *TP53* mutations fared better on everolimus than those without such mutations (48). *HRAS* mutations and *TP53* mutations are typically mutually exclusive in HNSCC (7). It will be interesting to determine whether the HRAS mutant cohort benefits from everolimus in combination with tipifarnib. In any case, recent encouraging reports showing durable responses in the small series of HRAS mutant patients with HNSCC treated with tipifarnib (49, 50) suggest that any new findings relevant to enhancing tipifarnib sensitivity and overcoming resistance will be welcomed for further clinical improvement of this difficult disease.

Authors' Disclosures

M. Pierobon reports personal fees from Theralink outside the submitted work. E.F. Petricoin reports personal fees and other support from Perthera, Inc., Theralink Technologies, Inc., and Ceres Nanosciences, Inc. outside the submitted work. C.J. Der reports grants and personal fees from Mirati Therapeutics and Deciphera Therapeutics; grants from SpringWorks Therapeutics; personal fees from Revolution Medicines, Ribometrix, Sanofi, Eli Lilly, Anchiano Therapeutics, and Turning Point Therapeutics outside the submitted work. A.D. Cox reports grants from NIH during the conduct of the study and has a patent for US7,838,531/8,257,915B2 issued. No disclosures were reported by the other authors.

Authors' Contributions

S. Javaid: Conceptualization, data curation, formal analysis, validation, investigation, visualization, methodology, writing–original draft, writing–review and editing. **A. Schaefer:** Conceptualization, data curation, investigation, visualization, methodology, writing–original draft, writing–review and editing. **C.M. Goodwin:** Data curation, formal analysis, visualization, writing–original draft, writing–review and editing. **V.V. Nguyen:** Investigation. **F.L. Massey:** Investigation. **M. Pierobon:** Resources, data curation, investigation, writing–review and editing. **D. Gambrell-Sanders:** Investigation. **A.M. Waters:** Data curation, formal analysis, investigation, writing–review and editing. **K.N. Lambert:** Investigation. **J.N. Diehl:** Formal analysis. **G.A. Hobbs:** Data curation, methodology, writing–review and editing. **K.C. Wood:** Resources, writing–review and editing. **E.F. Petricoin:** Resources, methodology, writing–review and editing. **C.J. Der:** Conceptualization, resources, supervision, funding acquisition, visualization, writing–original draft, writing–review and editing. **A.D. Cox:** Conceptualization, resources, supervision, funding acquisition, visualization, writing–original draft, project administration, writing–review and editing.

Acknowledgments

This work was supported by grants from the NIH to A.D. Cox, C.J. Der, and E.F. Petricoin (P01CA203657, R01CA42978 and R35CA232113). S. Javaid was

supported by a fellowship from the Royster Society of Fellows. C.M. Goodwin and G.A. Hobbs were supported by fellowships from the NIH (F32CA221005, F32CA200313, and T32CA009156, respectively). A.M. Waters was supported by a fellowship from the American Cancer Society (PF-18-061). J.N. Diehl was supported by fellowships from the Slomo and Cindy Silvian Foundation and the NIH (F30CA243253 and T32 CA071341).

The costs of publication of this article were defrayed in part by the payment of page charges. This article must therefore be hereby marked *advertisement* in accordance with 18 U.S.C. Section 1734 solely to indicate this fact.

Received February 13, 2021; revised August 16, 2021; accepted February 22, 2022; published first February 28, 2022.

References

1. Cox AD, Fesik SW, Kimmelman AC, Luo J, Der CJ. Drugging the undruggable RAS: mission possible? Nat Rev Drug Discov 2014;13:828–51.
2. Ahearn IM, Haigis K, Bar-Sagi D, Philips MR. Regulating the regulator: post-translational modification of RAS. Nat Rev Mol Cell Biol 2011;13:39–51.
3. End DW, Smets G, Todd AV, Applegate TL, Fuery CJ, Angibaud P, et al. Characterization of the antitumor effects of the selective farnesyl protein transferase inhibitor R115777 *in vivo* and *in vitro*. Cancer Res 2001;61:131–7.
4. Liu M, Bryant MS, Chen J, Lee S, Yaremko B, Lipari P, et al. Antitumor activity of SCH 66336, an orally bioavailable tricyclic inhibitor of farnesyl protein transferase, in human tumor xenograft models and wap-ras transgenic mice. Cancer Res 1998;58:4947–56.
5. Cox AD, Der CJ, Philips MR. Targeting RAS membrane association: back to the future for anti-RAS drug discovery? Clin Cancer Res 2015;21:1819–27.
6. Whyte DB, Kirschmeier P, Hockenberry TN, Nunez-Oliva I, James L, Catino JJ, et al. K- and N-Ras are geranylgeranylated in cells treated with farnesyl protein transferase inhibitors. J Biol Chem 1997;272:14459–64.
7. TCGA Network. Comprehensive genomic characterization of head and neck squamous cell carcinomas. Nature 2015;517:576–82.
8. Bray F, Ferlay J, Soerjomataram I, Siegel RL, Torre LA, Jemal A. Global cancer statistics 2018: GLOBOCAN estimates of incidence and mortality worldwide for 36 cancers in 185 countries. CA Cancer J Clin 2018;68:394–424.
9. Siegel RL, Miller KD, Fuchs HE, Jemal A. Cancer statistics, 2021. CA Cancer J Clin 2021;71:7–33.
10. Burtness B, Harrington KJ, Greil R, Soulières D, Tahara M, de Castro G., Jr., et al. Pembrolizumab alone or with chemotherapy versus cetuximab with chemotherapy for recurrent or metastatic squamous cell carcinoma of the head and neck (KEYNOTE-048): a randomised, open-label, phase 3 study. Lancet 2019;394:1915–28.
11. Kao HF, Lou PJ. Immune checkpoint inhibitors for head and neck squamous cell carcinoma: current landscape and future directions. Head Neck 2019;41:4–18.
12. Prior IA, Hood FE, Hartley JL. The frequency of Ras mutations in cancer. Cancer Res 2020;80:2969–74.
13. Braig F, Voigtlaender M, Schieferdecker A, Busch CJ, Laban S, Grob T, et al. Liquid biopsy monitoring uncovers acquired RAS-mediated resistance to cetuximab in a substantial proportion of patients with head and neck squamous cell carcinoma. Oncotarget 2016;7:42988–95.
14. Ho A, Chau N, Bauman J, Bible K, Chintakuntlawar A, Cabanillas ME, et al. Preliminary results from a phase II trial of tipifarnib in squamous cell carcinomas (SCCs) with HRAS mutations. Ann Oncol 2018;29:146O.
15. Zhou B, Ritt DA, Morrison DK, Der CJ, Cox AD. Protein kinase CK2α maintains extracellular signal-regulated kinase (ERK) activity in a CK2α kinase-independent manner to promote resistance to inhibitors of RAF and MEK but not ERK in BRAF mutant melanoma. J Biol Chem 2016;291:17804–15.
16. Baldelli E, Calvert V, Hodge A, VanMeter A, Petricoin EF 3rd, Pierobon M. Reverse phase protein microarrays. Methods Mol Biol 2017;1606:149–69.
17. Ozkan-Dagliyan I, Diehl JN, George SD, Schaefer A, Papke B, Klotz-Noack K, et al. Low-dose vertical inhibition of the RAF-MEK-ERK cascade causes apoptotic death of KRAS mutant cancers. Cell Rep 2020;31:107764.
18. Shalem O, Sanjana NE, Hartenian E, Shi X, Scott DA, Mikkelson T, et al. Genome-scale CRISPR-Cas9 knockout screening in human cells. Science 2014;343:84–87.
19. Taguchi Y, Schätzl HM. Small-scale triton X-114 extraction of hydrophobic proteins. Bio Protoc 2014;4:e1139.
20. Foucquier J, Guedj M. Analysis of drug combinations: current methodological landscape. Pharmacol Res Perspect 2015;3:e00149.
21. Ulsh LS, Shih TY. Metabolic turnover of human c-rasH p21 protein of EJ bladder carcinoma and its normal cellular and viral homologs. Mol Cell Biol 1984;4:1647–52.
22. Shi ZZ, Shang L, Jiang YY, Hao JJ, Zhang Y, Zhang TT, et al. Consistent and differential genetic aberrations between esophageal dysplasia and squamous cell carcinoma detected by array comparative genomic hybridization. Clin Cancer Res 2013;19:5867–78.
23. Hayes TK, Neel NF, Hu C, Gautam P, Chenard M, Long B, et al. Long-term ERK inhibition in KRAS-mutant pancreatic cancer is associated with MYC degradation and senescence-like growth suppression. Cancer Cell 2016;29:75–89.
24. Untch BR, Dos Anjos V, Garcia-Rendueles MER, Knauf JA, Krishnamoorthy GP, Saqcena M, et al. Tipifarnib inhibits HRAS-driven dedifferentiated thyroid cancers. Cancer Res 2018;78:4642–57.
25. Berndt N, Hamilton AD, Sebti SM. Targeting protein prenylation for cancer therapy. Nat Rev Cancer 2011;11:775–91.
26. Reid TS, Terry KL, Casey PJ, Beese LS. Crystallographic analysis of CaaX prenyltransferases complexed with substrates defines rules of protein substrate selectivity. J Mol Biol 2004;343:417–33.
27. Zverina EA, Lamphear CL, Wright EN, Fierke CA. Recent advances in protein prenyltransferases: substrate identification, regulation, and disease interventions. Curr Opin Chem Biol 2012;16:544–52.
28. Basso AD, Mirza A, Liu G, Long BJ, Bishop WR, Kirschmeier P. The farnesyl transferase inhibitor (FTI) SCH66336 (lonafarnib) inhibits Rheb farnesylation and mTOR signaling. Role in FTI enhancement of taxane and tamoxifen antitumor activity. J Biol Chem 2005;280:31101–8.
29. Castro AF, Rebhun JF, Clark GJ, Quilliam LA. Rheb binds tuberous sclerosis complex 2 (TSC2) and promotes S6 kinase activation in a rapamycin- and farnesylation-dependent manner. J Biol Chem 2003;278:32493–6.
30. Cox AD, Garcia AM, Westwick JK, Kowalczyk JJ, Lewis MD, Brenner DA, et al. The CAAX peptidomimetic compound B581 specifically blocks farnesylated, but not geranylgeranylated or myristylated, oncogenic ras signaling and transformation. J Biol Chem 1994;269:19203–6.
31. Prendergast GC, Davide JP, deSolms SJ, Giuliani EA, Graham SL, Gibbs JB, et al. Farnesyltransferase inhibition causes morphological reversion of ras-transformed cells by a complex mechanism that involves regulation of the actin cytoskeleton. Mol Cell Biol 1994;14:4193–202.
32. Suzuki N, Del Villar K, Tamanoi F. Farnesyltransferase inhibitors induce dramatic morphological changes of KNRK cells that are blocked by microtubule interfering agents. Proc Natl Acad Sci U S A 1998;95:10499–504.
33. de Morais EF, Rolim LSA, de Melo Fernandes Almeida DR, de Farias Morais HG, de Souza LB, de Almeida Freitas R. Biological role of epithelial-mesenchymal-transition-inducing transcription factors in head and neck squamous cell carcinoma: a systematic review. Arch Oral Biol 2020;119:104904.
34. Shibue T, Weinberg RA. EMT, CSCs, and drug resistance: the mechanistic link and clinical implications. Nat Rev Clin Oncol 2017;14:611–29.
35. Diaz AA, Qin H, Ramalho-Santos M, Song JS. HiTSelect: a comprehensive tool for high-complexity-pooled screen analysis. Nucleic Acids Res 2015;43:e16.
36. Brill S, Li S, Lyman CW, Church DM, Wasmuth JJ, Weissbach L, et al. The Ras GTPase-activating-protein-related human protein IQGAP2 harbors a potential actin binding domain and interacts with calmodulin and Rho family GTPases. Mol Cell Biol 1996;16:4869–78.
37. Xu L, Shao Y, Ren L, Liu X, Li Y, Xu J, et al. IQGAP2 inhibits migration and invasion of gastric cancer cells via elevating SHIP2 phosphatase activity. Int J Mol Sci 2020;21:1968–82.
38. Chatterjee S, Behnam Azad B, Nimmagadda S. The intricate role of CXCR4 in cancer. Adv Cancer Res 2014;124:31–82.
39. Gualberto A, Scholz C, Janes MR, Kessler L, Raza A. The CXCL12/CXCR4 pathway as a potential target of Tipifarnib in acute myeloid leukemia and myelodysplastic syndromes. Blood 2017;130:3957.
40. Bryant KL, Stalnecker CA, Zeitouni D, Klomp JE, Peng S, Tikunov AP, et al. Combination of ERK and autophagy inhibition as a treatment approach for pancreatic cancer. Nat Med 2019;25:628–40.

41. Kinsey CG, Camolotto SA, Boespflug AM, Guillen KP, Foth M, Truong A, et al. Protective autophagy elicited by RAF→MEK→ERK inhibition suggests a treatment strategy for RAS-driven cancers. Nat Med 2019;25:620–27.
42. Hah JH, Zhao M, Pickering CR, Frederick MJ, Andrews GA, Jasser SA, et al. HRAS mutations and resistance to the epidermal growth factor receptor tyrosine kinase inhibitor erlotinib in head and neck squamous cell carcinoma cells. Head Neck 2014;36:1547–54.
43. Rampias T, Giagini A, Siolos S, Matsuzaki H, Sasaki C, Scorilas A, et al. RAS/PI3K crosstalk and cetuximab resistance in head and neck squamous cell carcinoma. Clin Cancer Res 2014;20:2933–46.
44. Gilardi M, Wang Z, Proietto M, Chillà A, Calleja-Valera JL, Goto Y, et al. Tipifarnib as a precision therapy for HRAS-mutant head and neck squamous cell carcinomas. Mol Cancer Ther 2020;19:1784–96.
45. Lee HW, Sa JK, Gualberto A, Scholz C, Sung HH, Jeong BC, et al. A phase II trial of tipifarnib for patients with previously treated, metastatic urothelial carcinoma harboring HRAS mutations. Clin Cancer Res 2020;26:5113–19.
46. Du W, Liu A, Prendergast GC. Activation of the PI3'K-AKT pathway masks the proapoptotic effects of farnesyltransferase inhibitors. Cancer Res 1999;59:4208–12.
47. Li Q, Mattingly RR. Restoration of E-cadherin cell-cell junctions requires both expression of E-cadherin and suppression of ERK MAP kinase activation in Ras-transformed breast epithelial cells. Neoplasia 2008;10:1444–58.
48. Nathan CAO, Hayes DN, Harismendy O, Flores J, Moore-Medlin T, Gutkind JS, et al. Multi-institutional randomized double-blind phase II trial of Everolimus vs. Placebo as adjuvant therapy in patients with locally advanced squamous cell cancer of the head and neck (SCCHN). Int J Radiat Oncol Biol Phys 2020;106:1116.
49. Caruso C. Tipifarnib targets *HRAS*-mutant cancers. Cancer Discov 2019;9:1637–38.
50. Ho A, Brana I, Haddad R, Bauman J, Bible K, Faugeras L, et al. Preliminary results from a phase 2 trial of tipifarnib in squamous cell carcinomas (SCCs) with HRAS mutations. Mol Cancer Ther 2019;18:Abstract nr PR08.